New prospects and techniques for matter wave interferometry with ions

G. Schütz[1], A. Rembold[1], A. Pooch[1], P. Schneeweiss[2], A. Rauschenbeutel[2], I.S. Hwang[3] and A. Stibor[1]

[1] Physikalisches Institut and Center for Collective Quantum Phenomena in LISA$^+$, Universität Tübingen, Auf der Morgenstelle 15, 72076, Tübingen, Germany
[2] Vienna Center for Quantum Science and Technology, TU Wien - Atominstitut, Stadionallee 2, 1020 Vienna, Austria
[3] Institute of Physics, Academia Sinica, Nankang, Taipei, Taiwan, Republic of China

E-mail: alexander.stibor@uni-tuebingen.de

PACS numbers: 03.75.Dg; 03.75.-b; 41.85.-p; 07.77.Ka; 03.65.Ta

Abstract. We present new developments and potential applications for the first ion-interferometer realized by Maier et al. [1, 2, 3, 4], that verified at the end of the last century biprism interference and diffraction of 3 keV helium ions. The design of the setup is based on a coherent field emission source, an electrostatically charged biprism wire as a beam splitter and a multi-channel plate detector. However, due to deficiencies of the coherent ion source in the setup of Maier et al., the interference signal was low, therefore long integration times had to be accepted. In addition, the production of a significant uncharged particle radiation produced a high background intensity. The rest of the instrument proved to have excellent electron and ion optical properties and a high mechanical and electrical stability.

Here we describe in detail the original setup and the major innovations to overcome the deficiencies. We introduce a novel single-atom metal tip [5] as a stable, coherent and monochromatic field emission ion source with high brightness. Furthermore, a custom-built fiber pulling rig is used for fabricating silica nanowires with a homogeneous and reproducible diameter in the 100 nm range. These silica nanowires are then gold coated in order to realize the biprism beam splitter. The application of a delay line detector allows for a spatial as well as temporal resolution of the ion signal.

Compared to neutral atoms and point-like electrons, ions combine the properties charge and inner structure. This feature together with the high expected ion signal due to the new source, opens up possibilities for novel quantum optical experiments concerning the dependence of the inner particle structure in the Aharonov-Bohm effect. Additionally, with such an ion interferometer the first direct proof of the electrostatic Aharonov-Bohm effect comes into reach of current technical possibilities.

1. Introduction

The development of the first matter wave interferometer for neutral particles about two decades ago [6, 7] indicated the enormous scientific as well as technical potential in the interference of heavy, massive particles. It was the beginning of a fast developing new field, leading to a number of outstanding fundamental precision experiments with atom interferometers, such as the exact measurement of the earth rotation [8] or the gravitational acceleration with an ultracold atomic fountain setup where the beam splitting is performed by laser Raman pulses [9]. Soon after interferometry of molecular dimers [10] and C_{70} fullerenes [11] followed. In those cases material gratings were used as the diffracting element. The significant influence of the van der Waals interaction between the grating and the molecules prevented these methods to be used to interfere particles with considerable higher masses. This boundary could be exceeded by the use of a standing light-wave grating [12, 13] to accomplish the current mass record of 6910 amu with complex biomolecules [14]. Parallel to the development of new atom interferometers, the field of Bose-Einstein condensation was found. It allowed various experiments involving the splitting and combining of clouds of coherent, ultracold atoms, revealing matter wave interference patterns with high contrast [15].

As a consequence of the great success of interferometers with neutral atoms, these efforts have been extended towards ions at the end of the last century, when a biprism interferometer for helium ions was constructed by Maier and Hasselbach [1, 2, 3, 4]. Unfortunately, the low brightness of the coherent field ion source of only $10^{12}\,\frac{\mathrm{A}}{\mathrm{m^2 sr Torr}}$ turned out to be the weak point in the design. Very long exposure times of 15 minutes had to be taken into account. However, the extraordinary mechanical and electrical stability of the setup made it possible to accumulate interference fringes and diffraction for 3 keV He^+ ions for the first time. Another problem that turned up in connection with the field ion source was the emission of uncharged particle radiation, presumably recombined excited helium ions, causing a large background sharply centred in the middle of the image intensifier. In order to see the interference fringes, the coherent ions had to be deflected electrically out of these zone towards the edge of the detector. The large background and the low signal in the setup of Maier et al. prevented further quantum optical experiments with ion matter waves. A second attempt to build an ion interferometer was made by Krenn et al. [16]. The device could not generate ion interferences due to the low count rate of the ion source.

In this article we describe our efforts to modify and reactivate the ion interferometer of Maier et al. [1, 2, 3, 4] with novel components to overcome the mentioned deficiencies and to realize an interferometer for intensive helium and hydrogen ion beams. In section 2 we explain the setup of the original ion interferometer of Maier et al. and mention the changes we performed in the modified version. The most important new enhancements are then discussed in detail in section 3. Those are the ion source, the

biprism beam splitter and the detector. Furthermore a modern vacuum system was installed and the cryostat to cool the ion source was optimized. Novel sources for ion field emission, namely single-atom tips (SAT) are available since some years [23], making it feasible to produce an intensive, coherent and monochromatic helium or hydrogen ion beam already at moderate emission voltages. Under ideal test conditions [22, 5], the signal rates are up to three orders of magnitude higher than the signal in the ion interferometer of Maier et al. [3]. However, such high count rates are not yet realized in the modified ion interferometer, but even a moderately improved signal would allow to work at a lower ionization gas pressure in the UHV-chamber. Since we assume the helium gas pressure of 10^{-4} mbar used in the interferometer of Maier et al. [3] was the reason for the high background, we expect a significantly improved signal-to-noise ratio with the new sources.
In the interferometer of Maier et al. the beam gets coherently separated by a fine biprism wire, which is a gold-palladium coated glass fiber manually drawn to diameters typically between 200-600 nm [3]. To decrease the uncertainty in the diameter of the installed biprism, we introduce in the modified interferometer an alternative fiber drawing technique. The biprism wire with a sub-micron diameter is realized by a gold coated silica nanowire which is fabricated from a standard optical glass fiber in a heat-and-pull process using a custom-built fiber pulling rig. Before coating, fiber diameters around 350 nm can be achieved.
The detection in the modified interferometer is performed by a delay line detector, with the advantage compared to older techniques to show not only a high spatial, but also a high temporal resolution on the nanosecond time scale. This is an important feature for future quantum optical approaches in the field of Aharonov-Bohm physics. The temporal information can also be applied to suppress long term drifts in the interference pattern.

After we estimated the expected coherent ion count rate in the modified ion interferometer, we propose in section 4 new quantum optical experiments that are feasible with this setup. The additional parameter charge and the internal structure of ions offer crucial advantages in comparison to interferometers for neutral atoms and open up the door for a class of novel quantum optical experiments. Well known techniques from electron beam manipulation and electron interferometry can be applied on ions, making it possible to guide, split and combine the charged matter wave and expand the resulting interference pattern to fit the detectors resolution. The advantages compared to the point-like electrons are the inner structure of the ions and the higher mass. The coherent ion beam can be created by field ionisation at a metal tip at high positive voltage. The ion energy can be well controlled and the velocity spread is extremely small [37, 22]. These conditions are ideal to perform Aharonov-Bohm physics with ions. In this article we therefore propose two experiments. The first one concerns the structure dependence of the ions in the magnetic Aharonov-Bohm effect and the second one the first direct proof of the electrostatic Aharonov-Bohm effect.

Furthermore such an interferometer should allow for experiments concerning laser excitation of inner quantum states, decoherence studies [17] and might enable for extremely sensitive sensors for rotations and accelerations [18].

The de Broglie wavelength along the beam direction for coherent helium ions, emitted from a SAT at 7.6 kV [5], is calculated to be only 0.16 pm. For the 3 kV helium emission from the supertip in the original setup of Maier et al. the wavelength was 0.26 pm [1, 2, 3, 4]. Comparing these values with the current interference record for massive particles, namely a wavelength of $\sim$ 1 pm for large organic molecules with a mass of 6910 amu [14], indicates, that the ion interferometer in the original version could interfere particles with a four times shorter wavelength. In the modified interferometer we aim to realize interferences with even shorter particle wavelength. The proof of matter waves with lengths an order of magnitude smaller compared to the current record for neutral molecules is feasible.

2. Experimental setup

2.1. Biprism interferometry

The principle of biprism ion and electron interferometry is demonstrated in fig. 1 [20]. A point-like ion or electron source illuminates coherently a fine and conducting biprism wire between two grounded electrodes. Applying a positive (for electrons) or negative (for ions) potential on the wire, all possible beam paths get deflected by the same angle. Therefore the separated matter waves combine again shortly after the biprism and interfere with each other. As a result, an interference pattern parallel to the biprism wire can be detected in the observation plane. The electrostatic biprism is therefore a matter wave analogon to Fresnel's glass biprism illuminated with visible light, as well-known from classical wave optics.

This basic and, for electrons, well understood and optimized scheme can also be applied on ions. The challenge in this approach is the extremely small de Broglie wavelength of the ions. It sets stringent limits on the source size, the biprism diameter, the electromagnetic shielding and the stability of the whole setup. The opening angle α of coherent emission can be assessed by the relation for the angular coherence constraint $d \cdot \alpha \ll \frac{\lambda_{dB}}{2}$ [19, 20], where d is the source size and λ_{dB} the de Broglie wavelength of the particle. Applying a novel Ir/W(111) SAT beam source, as proposed in chapter 3.1, yields the smallest source size possible. The emission area is only a single iridium atom, with a diameter of $\sim$ 0.3 nm [5]. The angular coherence constraint can therefore be best fulfilled with such a field ion emitter, even for short ion wavelengths. A distance between the beam source and the biprism wire of 12 cm (as used in the ion interferometer), an energy of the charged particle of 3 keV and the condition $d \cdot \alpha_{max} = \frac{\lambda_{dB}}{2}$, lead to an electron wavelength of $\lambda_{dB} = 22.4$ pm and a maximal coherently illuminated area at the biprism with a diameter of 4.8 mm. For helium ions, using the same parameters, the

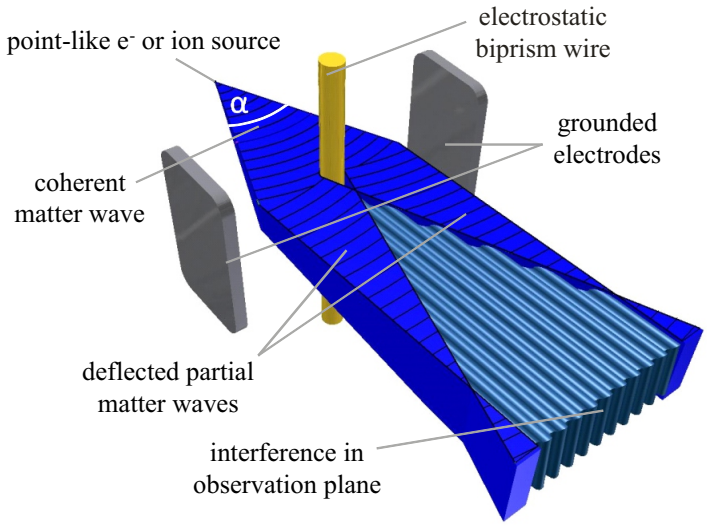

Figure 1. (Color online) The principle of biprism electron and ion interferometry [20]. A point-like source emits a charged matter wave in the coherence angle α. The matter wave is coherently divided by a fine electrostatically charged biprism wire between two grounded electrodes. The direction change of the two partial waves due to the electrical potential is the same at any radial distance R to the wire, since the field strength decreases with $1/R$, whereas the way the particles travel in the biprism increases with R. The deflection angle of the waves can therefore be adjusted by a change in the electrostatic voltage applied on the wire. If the separated waves do not overlap, a diffraction pattern can be observed at both biprism edges. If they do, the separated coherent beams interfere with each other in the observation plane.

matter wavelength is only 0.26 pm and the coherently illuminated region at the biprism is $\sim 56\,\mu$m. For C_{60} molecules at 3 keV the values are $\lambda_{dB} = 0.02$ pm and the coherent area at the biprism would be $\sim 4\,\mu$m. Certainly, to assure interference, the coherent region must be significantly larger than the diameter of the biprism wire, which can in principle be manufactured down to 100 nm, as it will be discussed in section 3.2.
Usual electron sources have emission areas with typical diameters of 1-2 nm, being much larger than a single atom, and resulting in a more incoherent beam. But not only the lateral coherence is necessary, also the temporal or longitudinal coherence length is important, which depends on the energy spread of the particles. The energy spread of the SAT for electrons is only 0.4 eV [22] and it is assumed to be of the same order of magnitude for ions.

2.2. Comparison between the original and the modified version of the ion interferometer

The setup of the modified biprism ion interferometer is shown in fig. 2. Originally the whole configuration besides the vacuum pumps was adopted from Maier et al. [1, 2, 3, 4]. Subsequently the following concrete modifications have been performed: The old ion beam source, a supertip (see section 3.1), was exchanged by a new one, a single-atom tip (SAT). A specially designed holder for the SAT, including a temperature diode, was

manufactured to combine it with a cryostat. The electric contacting of the tip was put inside the liquid helium bath of the cryostat to achieve lower temperatures. The biprism beam splitter was exchanged by a fiber drawn according to the new method described in section 3.2. For this beam splitter a new holder was manufactured. The holder together with the fiber were coated by a thin gold layer. In comparison to the interferometer of Maier et al., we varied hereby only the technique of biprism fiber production, leading to a more controlled way to reproduce a certain preset diameter. Additionally the CCD-phosphor detector was exchanged by a delay line detector as described in section 3.3. All the pumps in the vacuum system and the pressure sensor where renewed. As it was done in the original version [3], we installed in the modified interferometer a rotary vane pump in combination with a turbopump to achieve a pressure of 10^{-9} mbar, where the pumps can subsequently be disconnected by a slide valve and turned off to avoid contrast loss due to vibrations as discussed in section 2.5. In the interferometer of Maier et al., further pumping is provided by a titan sublimation pump and a cryopump. In the modified version, new pumps of these types and an additional ion getter pump was added to efficiently remove rest gas atoms. A new and extremely clean inlet pipe for the highly purified helium or hydrogen ionization gas was also applied. All electrical components within the UHV, besides the detector, were isolated from the electricity network and operated by batteries to prevent voltage or current fluctuations. In the original setup this was already realized for most of the electrical sources.

In the original and the new version of the interferometer, the distances between the SAT and the middle of the other components within the setup are: tip to 1st deflector: 11 mm, tip to movable MCP-detector: 29 mm, tip to 2nd deflector: 94 mm, tip to 3rd deflector: 118 mm, tip to biprism: 120 mm, tip to Wien filter: 195 mm, tip to image rotator: 220 mm, tip to quadrupole lenses: 260 mm, tip to delay line detector: 570 mm [3]. All components are in an ultra-high vacuum chamber with a pressure of 10^{-10} mbar before the ion emission starts. The vacuum system is optimized for helium and hydrogen pumping. During the experiment, the setup is floated with these gases to a pressure between 10^{-4} and 10^{-6} mbar. The gas is ionized by a metal tip at high voltage, forming a coherent ion matter wave. The beam source is cooled by a liquid helium cryostat. The differences between the applied tips in the original and the new version will be described in detail in section 3.1. The experience from electron interferometry indicates the necessity to build a small and compact interferometer with no mechanically moving parts directly interfering with the beam [21]. For that reason the whole interferometer is mounted on two rigid ceramic bars and the ion beam is aligned by three deflector electrodes. To characterize, prepare and adjust the ion source, a multi-channel plate (MCP) detector in combination with a phosphor screen can be moved into the particle beam. With the help of a 45 ° mirror, the screen can be seen through a side window in the chamber. After the ion beam emission is optimized, this detection unit will be moved out of the optical beam axis. Two deflectors adjust the beam towards the beam splitter. The ion matter wave is separated by the electrostatic biprism wire, realized by

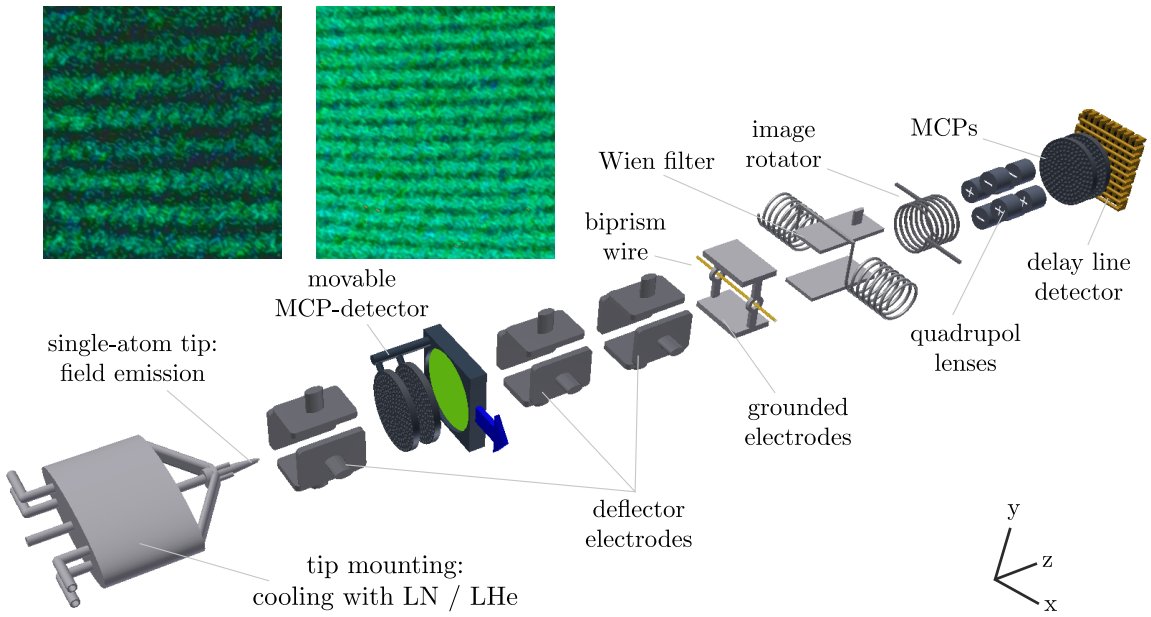

Figure 2. (Color online) The experimental setup of the ion interferometer based on [1, 2, 3, 4]. All modifications compared to the original version by Maier et al. are explained in the text. The ion or electron source is an Ir/W(111) single-atom tip (SAT) [5] cooled by a liquid helium cryostat. After the first deflector electrode for beam aligning, the particles get detected by a movable MCP-detector. This part together with a phosphor screen, forms a field electron or field ion microscope, which is important to verify the creation of a pyramidal shape of the SAT. Afterwards the MCP-detector is moved out of the optical axis and the ion beam is aligned onto the biprism by two further deflector electrodes. The biprism separates the beam coherently and overlaps the two partial waves. The Wien filter restores the longitudinal coherence. The partial matter waves combine again and form an interference pattern which is oriented along the x-axis of the quadrupole lenses by the image rotator. The quadrupole lenses magnify the image in the y-direction. At the end, the ions or electrons get detected by a combination of two MCPs and a delay line anode. **Inset:** First interferograms with electrons at two different biprism voltages to test the modified interferometer. Here the detection was still performed by a phosphor screen instead of the delay line detector. A clear electron interference pattern is visible, proofing the good surface quality of the biprism, manufactured by the new fiber drawing technique described in section 3.2.

a gold coated silica nanowire as described in section 3.2 [24, 26]. It is positioned in the middle between two grounded electrodes that are 4 mm apart from each other.

2.3. The Wien filter

Before the partial waves are detected, they pass a Wien filter. This device, described in detail in [28], consists of two magnetic coils in combination with two deflector electrodes. The installation of a Wien filter was already necessary in interferometers for slow electrons and is even more crucial for ions. It corrects the wave package shift caused by the deflector electrodes after beam alignment and is able to restore and measure

the longitudinal coherence. Due to its finite energy distribution, the source emits a range of de Broglie wavelengths that overlap and appear as wave packages. Within the interferometer, the two partial waves enter the field of the deflector electrodes. Since they are at different positions inside the electrodes, they are exposed to unequal potentials and propagate with different group velocities. This causes a longitudinal shift between the packages. If the shift is longer than the longitudinal coherence length, the wave packages do not overlap any more in the detection plane and no interference can be observed. In the Wien filter, an electric and magnetic field is created both perpendicular to each other and to the path of the beam. The field strengths are set such, that the electric and the magnetic forces on the electrons or the ions cancel each other. Therefore the Wien filter does not deflect the beam or causes any phase shift on the wave packets. It can be adjusted in a way, that the wave package delay due to the deflector electrodes can be exactly compensated and full longitudinal coherence is restored [28].
After the Wien filter, the ion beam encounters an image rotator. It is a coil with a magnetic field parallel to the direction of propagation, that induces a force on the ion's transversal velocity component and rotates the interference pattern. It is necessary for the alignment of the pattern towards the axis of the quadrupole lenses for image magnification.

2.4. Interference pattern magnification

For the described interferometer, the distance between two mutual interference fringes is on the order of several nanometers. The exact value depends on the geometry of the interferometer, the biprism voltage and the wavelength of the particles. At higher biprism voltages the angle of the overlapping partial waves in the detection plane is larger, leading to a smaller distance between two interference maxima. The applied commercial MCP has a resolution of about 100 µm. The task of the lens system is therefore to magnify the interference pattern in the direction orthogonal to the biprism wire axis (y-direction, see fig. 2) by a factor of about $m_y = 10^4$ to 10^5 by still remaining a rather small magnification m_x along the direction of the interference stripes (x-direction). The latter would only cause a loss in signal strength. This is achieved by using quadrupole lenses as simulated in fig. 3 by [3]. The possibility to expand the interference pattern by quadrupole lenses is one of the important advantages of interferometry with charged particles in comparison to neutral ones.
The lenses are composed out of four cylindric electrodes, arranged towards each other quadratically and parallel towards the beam path. Two diagonal opposing electrodes have the same, the other two the opposite polarity. The calculations for fig. 3 indicate, that the best results can be achieved by two quadrupoles in a small distance towards each other. With this arrangement, magnifications up to 10^5 orthogonal and in the order of ten parallel to the interference pattern can be achieved, respectively.

The last component in the setup of fig. 2 is the MCP-detector with a delay line

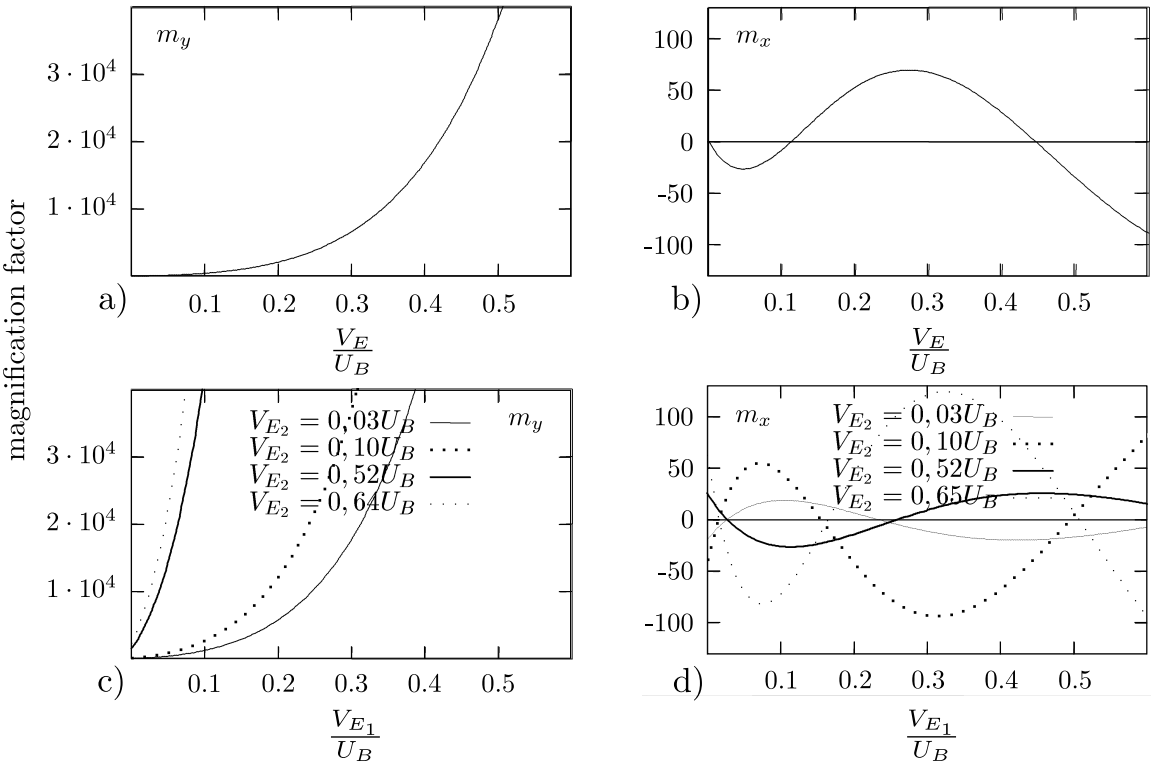

Figure 3. Simulations of the quadrupole image magnification in the ion interferometer, performed using transfer matrices [30, 31] according to the geometrical design and the electrostatic potential of the electrodes (data taken from [3]). In a) the magnification of a single quadrupole lens is simulated for the y-direction in b) for the x-direction. V_E accounts for the voltage of two opposing cylindrical electrodes in the quadrupole. The other two are arranged in a 90° angle towards them with an impressed voltage of $-V_E$. These values are normalized with respect to the ion acceleration voltage of the source U_B. The oscillatory behaviour in the x-direction can be suppressed by an additional quadrupole lens after a distance of 10 mm. The resulting magnification on the detector is simulated in c) and d) for both directions and different voltages V_{E_1} and V_{E_2} for the first and second quadrupole, respectively.

anode. This component is an important improvement to the interferometer of Maier et al. [3, 4] and to other biprism electron interferometers as it will be discussed in section 3.3. The polarity of all components can be reversed to change from ion to electron interferometry. This convenient feature can be used to optimize the beam path since the electrons have a larger de Broglie wavelength and interference is easier to achieve.

2.5. Prevention of mechanical and electromagnetic noise

Great care has to be taken to avoid a loss of interference contrast due to vibrations of the building that houses the laboratory with the ion interferometer. It is known from neutral molecule interference [32] that especially the influence of low frequency vibrations in the acoustic regime between 50 and 1000 Hz can wash out the interference pattern, since it induces a phase shift during signal integration. For that reason, the interferometer

configuration is based on a rigid design known from biprism electron interferometry [21], where low resonance frequencies within the apparatus are avoided. Electron interference measurements with varying biprism deflection angles in the original interferometer of Maier et al. indicate, that rotating pumps decrease the contrast, due to their vibrations. The results are shown in fig. 4 [3]. Due to the slow velocity of ions compared to electrons it is assumed, that the contrast loss will be even higher. Therefore it was necessary to disconnect these pumps by a valve before an ion interference pattern is recorded and maintain the vacuum by pumps without rotating components.
Cooling the beam source with liquid helium could also be a possible channel to introduce noise due to mechanical vibrations if the cooling liquid is boiling. To avoid these kind of vibrations, a good heat shield, cooled by liquid nitrogen, was provided in the original and new setup, assuring steady state conditions without boiling.

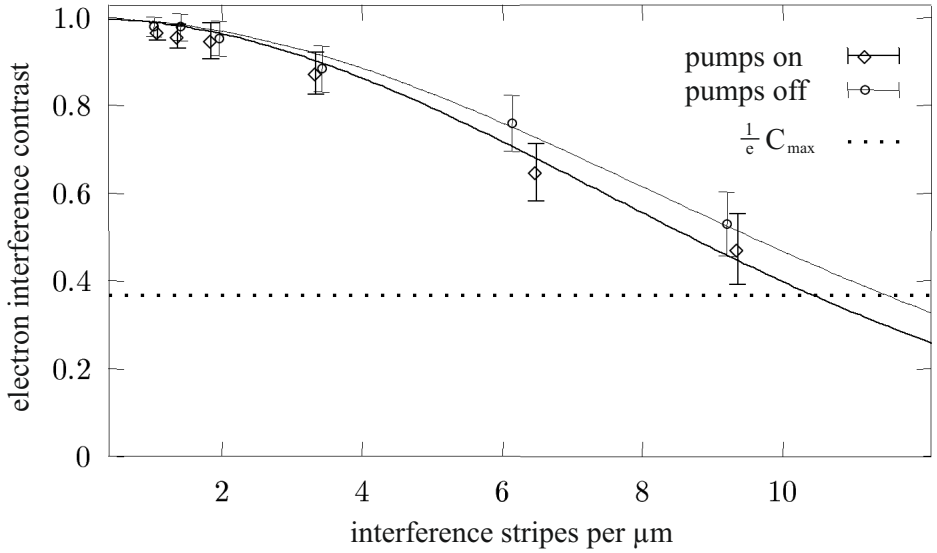

Figure 4. Effect of mechanical vibrations from the turbo- and rotary vane pump to the electron interference contrast for 2 keV electrons in the original ion interferometer of Maier et al. (data taken from [3]). For the determination of the contrast an average over 10 stripes was calculated. A clear influence of the mechanical vibrations by the pumps to the interference contrast can be observed. Generally the contrast decreases with decreasing distance between two interference maxima. The latter is the result of scanning the deflecting biprism voltage. The number of stripes per µm is given without quadrupole magnification, which was deducted from the measurements.

Due to the fact, that charged particles are interfered, electromagnetic noise can influence the phase of the ions, leading to a decreasing contrast. From electron interferometry it is known, that this kind of noise has an important influence and great care needs to be taken to shield the beam path. Therefore the interferometer is screened inside the vacuum chamber against external electric and magnetic fields by a copper and a mumetal tube. All apertures and deflector electrodes inside the interferometer are made out of titanium, due to its favourable paramagnetic properties. As mentioned, all the electronics for beam manipulation are disconnected from the power grid and

supplied by batteries to avoid 50 Hz noise and voltage fluctuations. This was mainly realized already in the original interferometer, where voltage and current supplies were measured to show a relative stability level and a temperature drift between 10^{-5} and 10^{-6} [3]. Additionally, the whole experiment together with the electronics are put inside a metal cabin to be shielded against electromagnetic noise, mainly from microwave and radio frequencies.

3. New components in the modified ion interferometer

3.1. The ion source: Single-atom tip (SAT)

The choice of the optimal beam source with a highly coherent signal is crucial for an ion interferometer, that allows sophisticated future quantum optical experiments. The lateral and longitudinal coherence length, the emission angle, the signal intensity and the spatial stability depends on the beam source. An established technique to produce coherent ion beams is to etch a tiny metal tip and put it on high voltage in vacuum. Then, gas atoms are streamed towards the tip. Since the electrical field gradient is highest at the region with the strongest curvature, the atoms get ionized only at the tip end and accelerated towards the biprism. Observing the ions with a MCP-detector realizes a field ion microscope, a common method to observe even single atoms on the surface of the tip [41].
Several different tip types have been developed in the last decades. The electron emission characteristic of four of them are listed in tab. 1. In the first one, electrons are thermally emitted by a comparably blunt tungsten or lanthanum hexaboride (LaB_6) tip. Typical diameters are between 20 and 400 µm, and common tip temperatures are about 2000 K. The electrons emitted by the tip are accelerated towards a counter electrode due to an applied electrostatic field [33]. The second type describes an etched tip with a diameter below 100 nm where the electrons get extracted by field emission. This type was commonly used for electron interferometers. The third one, the so called "supertip", is an etched tip, where a tiny ~ 1 nm protrusion is created by a certain technique [43]. This was the ion source in the original interferometer of Maier et al. [3]. Due to this geometry the emitted electron or ion matter wave experience a self focusing effect. An ion beam is emitted with a high angular confinement of about 2 °, instead of about 60 ° full emission angle for conventional field emission tips [36]. However, Maier et al. stated [3], that this protrusion, and therefore the ion emission center, is unfortunately spatially only stable for about one hour, with a large uncertainty between different tips. This is a disadvantage for the use in ion interferometry, since the beam alignment before signal acquisition needs typically longer than this time.

The best choice for ion interferometry is potentially the fourth emitter type, the recently developed SAT [22, 23]. As it is illustrated in fig. 5, these tips are etched from a single crystal (111) tungsten wire and covered with a monolayer of iridium. After

	Thermal emission	Etched tip	Supertip	SAT
Source diameter	20-400 µm [33]	0.2 µm [33]	4 nm [34]	3 Å [5]
Electric field [V/m]	5×10^8 [33]	10^9 [33]	10^{10}[34]	5×10^{10} [35]
Energy spread [eV]	$0.5 - 2$ [33]	0.2 [33]	0.5 [36] (ions: 1 [37])	0.4 [22]
Max. brightness [A/m^2 sr]	10^9 [33]	10^{13} [33]	$10^{13} - 10^{14}$ [36] (ions: 10^{15} [40])	$10^{13} - 10^{14}$ [38, 39] (ions: 3×10^{15} [5])

Table 1. Comparison of different emission sources for electron field emission. The data in brackets refer to helium ions with 1 Torr ionizing gas pressure. Here "etched tip" relates to a blank tungsten tip without an artificial protrusion as generated on the "supertip". The source size for SAT of 3 Å takes into account, that only the topmost iridium atom ionizes the gas molecules and is therefore the origin of the beam.

installation into ultrahigh vacuum the tip is electrically heated for several times to a temperature between ~ 1053 and 1083 K for 30 to 60 seconds. The temperature of the SAT welded on a 130 µm tungsten wire can be measured accurately by a disappearing-filament-pyrometer. Due to surface energy optimization, the tip forms a three-sided atom pyramid. It could be shown, that the tip apex is a single iridium atom [22]. Applying a high voltage, the largest field gradient is above the topmost atom. It is therefore the origin of the ion beam after field ionization of inflowing gas atoms (He, H_2). The field emission pattern is observed on the movable MCP-detector. The pyramidal shape can be regenerated in vacuum over 50 times by annealing [5]. The SAT can be used for electron and ion emission by applying voltages with different polarities of a few hundred volts for electrons and 3 to 10 kV for ions. For maximal helium ion emission a voltage of ~ 7.8 kV should be applied at a gas pressure of $\sim 10^{-5}$ mbar [5]. The small source size of ~ 0.3 nm [5] results in an extremely coherent ion beam. However, it cannot be excluded, that for very high ionization voltages the atoms may get already ionized on the shank of the pyramid, causing a decrease of spatial coherence. Field ion microscopy imaging of the beam origin is not possible for high count rates due to signal saturation in the detector. Cooling the SAT from a temperature of 80 K to 20 K increases the helium ion emission by a factor of 10 [5]. For that reason, the tip is mounted in the ion interferometer on a liquid helium cooled cryostat. The increased count rate minimizes the integration time for the interference pattern.

As indicated in tab. 1, a maximal He^+ beam brightness of $3 \times 10^{15} \frac{\mathrm{A}}{\mathrm{m^2 srTorr}}$ could be achieved for an iridium covered SAT at a voltage of 7.6 kV under test conditions by [5]. For H_2^+ molecules the maximal brightness was even higher at a lower ionization voltage of 3.8 kV, namely $1.3 \times 10^{16} \frac{\mathrm{A}}{\mathrm{m^2 srTorr}}$ [5]. However, these values have not been reproduced inside the ion interferometer yet, further source optimization is still necessary. As for the supertips, a self focusing effect (see fig. 5) limits the emission angle to 1.5 °. The

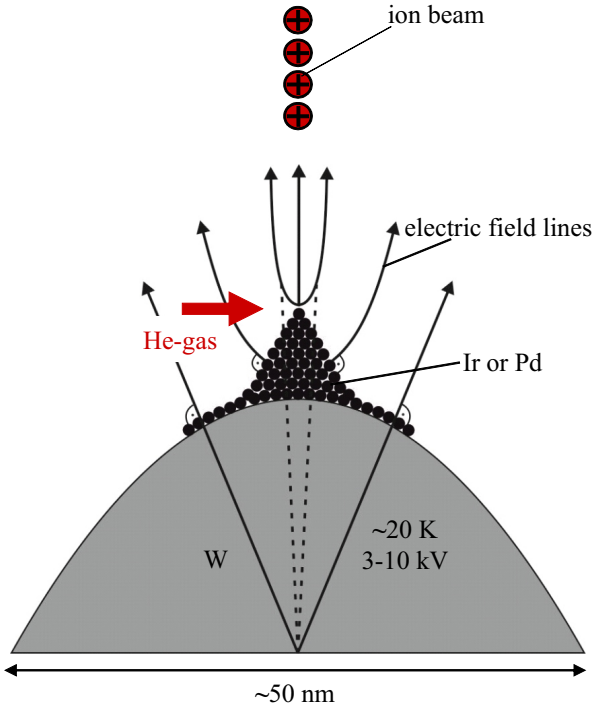

Figure 5. (Color online) Sketch of a field ion emission from a SAT as a coherent emission source for ion interferometry. The tip manufacturing procedure was first accomplished by [23] and improved by [22, 5]. A monolayer of iridium is deposited on an etched tungsten tip. After annealing, a 3-sided atom pyramid forms, that is set on a high voltage. Then gas atoms are streamed in, get ionized at the topmost atom and are accelerated along the interferometers beam path. The arrows indicate the direction of the electric field lines orthogonal to the tip surface. Since lines cannot cross, the ones orthogonal to the pyramid surface bend towards the center, resulting in a self focusing effect and an ion emission into a solid angle of $\sim 1.5\,^{\circ}$.

long time stability of these SAT sources is extraordinary high, variations of 3 % for helium and 5 % for hydrogen for about 30 minutes have been measured, and they do not show any degradation after a total operation time of 80 hours [5].

As mentioned, the field source used in the original ion interferometer of Maier et al. [1, 2, 3, 4] was a supertip. It revealed not to be practical for further, more complicated quantum-optical experiments, due to its low brightness and high background radiation. According to literature [40, 44], a larger brightness by two to three orders of magnitude was expected, but could not be verified in the experiment. The reasons for these variations are unknown. The maximal helium beam brightness achieved in the original version of the ion interferometer was about $10^{12}\,\frac{\mathrm{A}}{\mathrm{m^2 srTorr}}$ at $\sim 3\,\mathrm{keV}$ [3]. The beam source was cooled by liquid nitrogen. Subsequent attempts to improve the brightness by cooling the field emitter with liquid helium were successful [42] and will be applied in the modified ion interferometer. Another deficiency of the Maier et al. setup was the mentioned spatial instability of the artificial protrusion. The beam origin moved during signal acquisition for most applied supertips. Since long integration times were

required, the instability led to uncorrelated phase shifts, destroying the contrast. However, one exceptional protrusion was stable for about two hours, enough time for beam alignment and to record helium ion interference and diffraction with an integration time of 15 minutes for each pattern [1, 2, 3, 4]. The tip got destroyed in the subsequent effort to interfere also hydrogen ions.

3.1.1 Expected coherent ion count rates with the new SAT-source

Since the SAT source is one of the key innovations in the modified ion interferometer, we now estimate the expected amount of coherent ions on the detector. This is necessary to infer the feasibility of the device for more sophisticated future quantum optical experiments, that have not been possible with the setup of Maier et al. The iridium SAT at a temperature of 20 K, has a beam brightness of $1.3 \times 10^{16} \frac{\mathrm{A}}{\mathrm{m^2 sr Torr}}$ for hydrogen ions accelerated with an emission voltage of $U = 3.8\,\mathrm{kV}$ and $3 \times 10^{15} \frac{\mathrm{A}}{\mathrm{m^2 sr Torr}}$ at $U = 7.6\,\mathrm{kV}$ for helium ions [5]. Applying a gas pressure of 10^{-5} mbar in the UHV chamber leads to an ion emission of $E_0 = 9.8 \times 10^{10} \frac{\mathrm{A}}{\mathrm{m^2 sr}}$ for hydrogen and $E_0 = 2.3 \times 10^{10} \frac{\mathrm{A}}{\mathrm{m^2 sr}}$ for helium ions.
Certainly, only a small fraction of these ions are emitted in the coherently illuminated area. This fraction is determined by the already mentioned angular coherence relation $d \cdot \alpha \ll \frac{\lambda_{dB}}{2}$, defining the maximal emission angle in which the ions are still coherent, $\alpha = \frac{\lambda_{dB}}{2 \cdot d}$ (see fig. 1). With this angle, the coherently illuminated area in the detection plane with a radius l_k just before quadrupole magnification can be determined. The coherently emitted ions contribute to the interference pattern which is then magnified in the x and y-axis by the magnification factors m_x and m_y (see simulations in fig. 3). The signal is recorded on the active detector area A_{det} with an efficiency P_N. The number of coherent ions I_k per second on the detector is deduced in [3] and follows the relation

$$I_k = \frac{2 P_N \, A_{det} \, E_0 \, \lambda_{dB}^2}{m_x \, m_y \, l_k^2 \, \pi \, e} \quad . \tag{1}$$

Using the mentioned parameters in the interferometer of Maier et al. with supertips, a maximal count rate of ~ 50 coherent helium ions per second is expected [3]. In the modified version of the ion interferometer, due to the larger ion emission of the SAT, a maximal signal of $\sim 6.1 \times 10^3$ coherent helium ions per second are expected at a gas pressure of 10^{-5} mbar and for an ion acceleration voltage of 7.6 kV. For hydrogen H_2^+-dimers at 3.8 kV the coherent signal is calculated to be even higher, namely $\sim 2.7 \times 10^4$ ions per second. The significantly larger signal rate allows for integration times for an ion interference pattern of only seconds.

3.2. The beam splitter: A new method for biprism preparation

The electrostatic biprism is the core element in the ion interferometer, since it acts as a coherent beam splitter for the charged matter wave. It needs to be electrically conducting. Furthermore it is crucial that the biprism has a smooth surface with a roughness in the nanometer range and a diameter well below 1 µm over a length of at least 4 mm. Due to these requirements it is not practical to use a metallic wire. The usual technique to manufacture such thin wires in electron interferometers as well as in the original ion interferometer of Maier et al. was to manually draw a glass fiber out of a silica rod above a hydrogen-oxygen flame [3, 20]. The technique needed a lot of experience and could produce wires with typical diameters between 200 and 600 nm [3]. Subsequently a small gold layer with a thickness of 20 to 30 nm was evaporated on the surface. In some cases two layers of different metals, such as gold-copper, gold-silver or gold-palladium were deposited to avoid deformation of the interference pattern due to cracks in the gold layer. The disadvantage of this method was, that the diameter of the wire varied from one preparation to the other significantly, sometimes by several hundred nanometers. Since great care had to be taken to avoid dust deposits, the wire had to be immediately inserted into the vacuum chamber after preparation. A prior measurement of the diameter in a scanning electron microscope (SEM) was not possible, since the biprism got contaminated due to the pumping procedures in the apparatus. Therefore, no exact information about the diameter was available, leading to a significant uncertainty that enters the analysis of the interference data.

As a further development in the modified ion interferometer, we introduce a biprism preparation procedure, where a certain diameter can be chosen and reliably be reproduced without further SEM analysis of each newly created fiber. This is especially important for the upcoming data analysis of the expected ion interference pattern, where the biprism diameter influences the deflection angle and must be significantly smaller than the coherently illuminated zone at the biprism. For that reason, a custom-built computer-controlled fiber-pulling rig [25, 26] was employed to fabricate biprism wires for the modified ion interferometer. For the heat-and-pull process, a standard optical fiber is attached on two linear translation stages and positioned above an hydrogen-oxygen flame with a stoichiometric gas mixture. The softened fiber is stretched and at the same time translated with respect to the flame along its axis. With that technique, tapered optical fibers with pre-defined shape can be created [27]. For the biprism beam splitter fabricated here, this radius profile consists of a nanowire section with a homogeneous nominal diameter of 350 nm and a length of 6 mm that is linked to the unprocessed fiber ends by two tapered fiber sections. The corresponding nominal radius profile is presented in fig. 6. Using SEM-measurements, it was shown that the actually realized fiber-profiles deviate by less than ± 10 % from the intended design [27]. With this technique it is possible to produce fibers with a diameter down to about 100 nm [27]. In order to test if this procedure can be applied for the creation of an ion

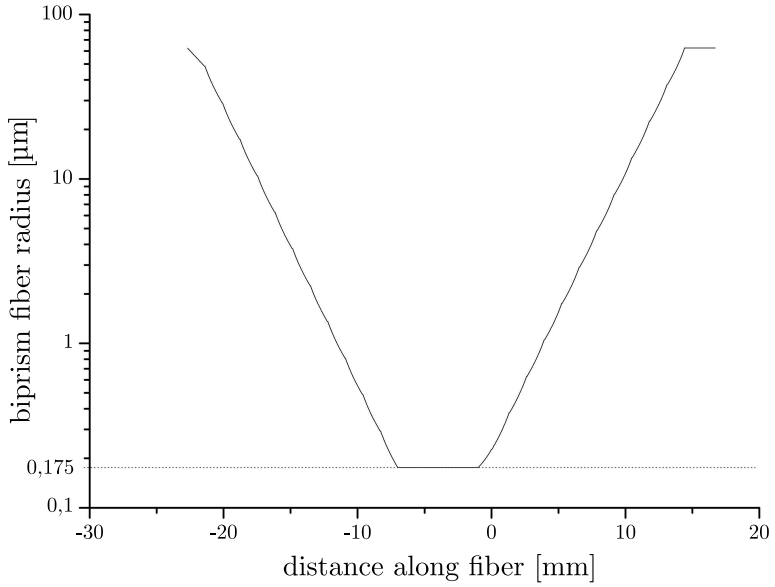

Figure 6. Nominal fiber radius-profile of the uncoated biprism wire for the modified ion interferometer. The nanowire-section has a nominal diameter of 350 nm, over a length of about 6 mm.

interferometer biprism, two fibers were pulled as described and fixed on an U-shaped titanium mount with ultra-high vacuum compatible glue. Thin layers of gold were subsequently deposited on the fibers with different sputtering times. To prevent effects related to contact potentials, the holders and the grounded electrodes were sputtered as well. To ensure a constant coverage on all sides of the biprism, the probes were rotated during the sputtering process by a stepper motor. Fig. 7 shows SEM images of the resulting biprism wires. The diameters including the gold layer inferred from these images are 388 nm and 435 nm. Based on the nominal diameter of the silica nanowires of 350 nm, we estimate the gold layers to have a thickness of $\sim$ 19 nm and $\sim$ 43 nm, respectively. The uncertainty in these values are yet not identified. We tested a biprism wire with the same manufacture parameters as the one in fig. 7 a) in the modified version of the ion interferometer with electron matter waves. Two resulting electron interference pattern for different biprism voltages are presented in the inset of fig. 2 proofing the good quality of the beam splitter.

3.3. The delay line detector: Spatial and temporal resolution of the interference fringes

The delay line anode in the modified ion interferometer replaces the fluorescent screen in the version of Maier et al [3]. The anode is composed out of a mesh of horizontal and vertical installed blank wires and arranged behind two MCPs [53]. After an ion or electron impact, the MCPs generate an amplified electron pulse, which is the starting

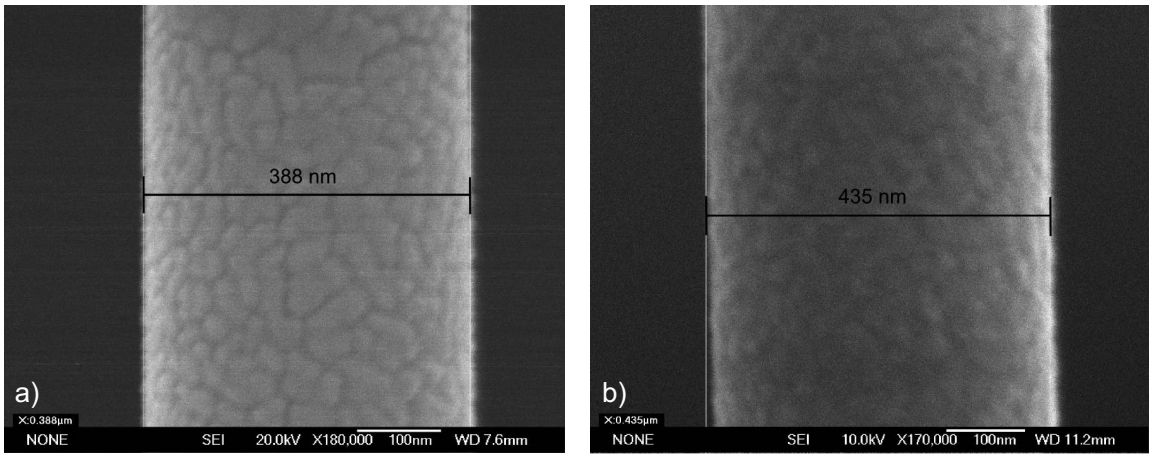

Figure 7. SEM images of two biprism wires based on gold coated silica nanowires. Both bare silica nanowires had a nominal diameter of 350 nm and were coated with gold for different sputtering times. The resulting layer thicknesses are estimated to be 19 nm in a) and 43 nm in b). The low roughness of the gold surface inferred from the image is an important requirement for the biprism wire to be used as a beam splitter in ion interferometry.

point of two pulses in each anode wire, propagating in opposite directions. Measuring the time of arrival at both ends of each wire with nanosecond accuracy allows for the determination of the starting point, therefore a spatial and temporal resolution of the impact events.

This is an advantage compared to the original interferometer of Maier et al., since the fluorescent screen could not provide a temporal resolution. In the modified version, this information can be used to suppress the influences of long term drifts of the interference pattern. Drifts arise due to mechanical or electrical instabilities, causing a phase shift of the whole interferogram. The accumulation of an interference pattern, that lasts longer than those drifts will therefore decrease the contrast. With the new detector, it is possible to correlate two consecutive detection events [29] and remove this contrast loss due to drifts for time scales longer than the time between the events. Let us assume, that two interference maxima in the detection plane are separated by a distance L with respect to each other in the direction orthogonal to the stripes (y-direction in fig. 2). If an ion is detected within one of these maxima, it is more likely for a subsequent ion to hit the screen in a distance of multiples of L, therefore in another maxima. Plotting the y-distances between two successive ions on the detector versus the rate of events with this particular spatial separation, yield a periodic curve with maxima and minima. It has a periodicity of L, revealing a significant pattern that proves interference. Since this correlation method takes only the time between two events into account, drifts with longer timescales will drop out. As it will be discussed in section 3.1.1, we expect an ion count rate in the kHz-regime with the SAT-source. The delay line detector can therefore potentially remove any phase drifts with timescales longer than milliseconds. It will make even long integration times for sophisticated quantum optical experiments

possible.

Another advantage of the new delay line detector is the ability to correlate the incoming ions to an external reference signal with a resolution of about one nanosecond. This is especially important for the proposed first direct proof of the electrostatic Aharonov-Bohm effect with such an ion interferometer, that will be discussed in section 4.5. It is additionally convenient to have the whole detection unit inside the vacuum. With the fluorescent screen, the light had to be transferred by glass fibers outside the vacuum chamber and was recorded by a camera. In such a detection scheme, more care had to be taken to avoid additional noise or signal losses.

4. Perspectives for the modified ion interferometer: Aharonov-Bohm physics with ions

In the famous paper of Aharonov and Bohm [45], two experiments are proposed to proof that the influence of vector and scalar potentials have a direct physical effect on the phase of charged particles, even in absence of any magnetic or electric field. Their predictions are known as the magnetic and the electrostatic Aharonov-Bohm effect. Shortly after, this phase shift could be demonstrated for the vector potential with an electron biprism interferometer [46]. The experiment proved the magnetic Aharonov-Bohm effect and showed impressively that potentials are not only mathematical constructs to create fields, as it was widely believed at that time, but seem to be even more fundamental.

The proposed Aharonov-Bohm effects are only accessible for charged particles and yet only the magnetic Aharonov-Bohm effect could be proven with point-like electrons [46]. There are speculations that ions could in principle show a different behavior, since they have an inner structure [47]. Moreover, the electrostatic Aharonov-Bohm effect has not been proven to date directly, such as it was proposed in the original paper, without the particle exposed to any field. The reason is, as we will explain in section 4.2, that the electrons are too fast to perform such an experiment. However, for the much heavier and therefore slower ions this proof of principles comes into reach with modern ultra-fast puls-generators and detectors. In the next sections we propose two experiments to test the magnetic and the electrostatic Aharonov-Bohm effect with the modified ion interferometer.

4.1. The magnetic Aharonov-Bohm effect

In the first proof of the magnetic Aharonov-Bohm effect with electrons by Möllenstedt et al. [46], a combination of two biprism allowed a 60 µm beam separation, far enough to install a tiny 14 µm magnetic coil in between. The situation is illustrated in fig. 8 a). The magnetic field inside the coil is given by the relation $B = \mu_0 \frac{N}{L} I$ with N being the number of coil windings, L the length of the coil and I the current. In a

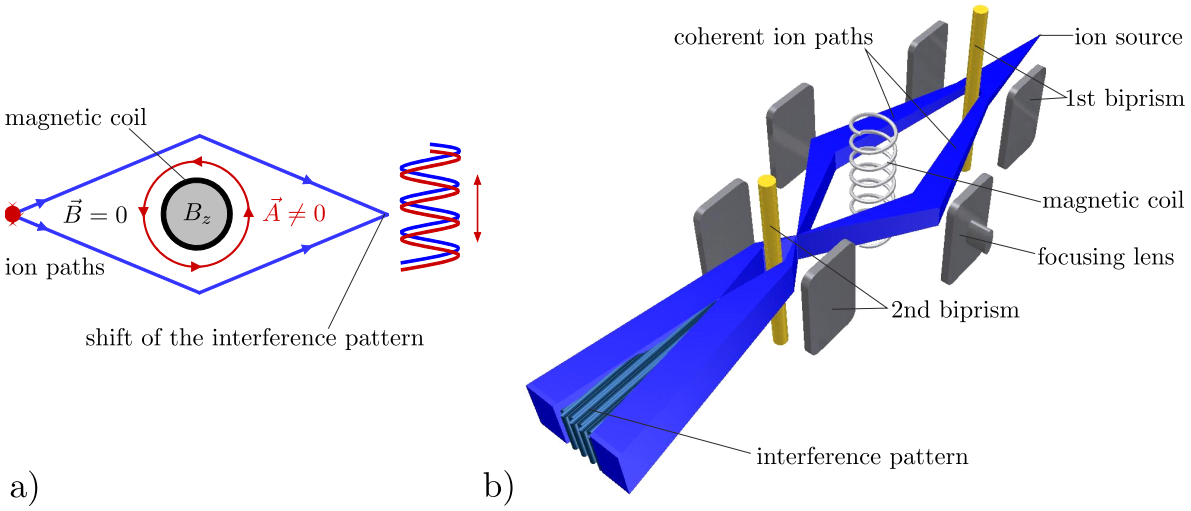

Figure 8. (Color online) Proposed measurement of the magnetic Aharonov-Bohm effect with ions. a) As originally suggested by Aharonov and Bohm [45] the beam is split into two coherent partial waves. They pass a magnetic coil with a magnetic field that is nonzero inside (B_z) and zero outside close to the coil. The ions interact only with the nonzero vector potential $\vec{A}$, which points in opposite direction for different paths. This causes a phase shift in the interference pattern depending on B_z. b) Proposed experimental realization with ions. To insert a micro coil between the separated partial waves, the beam has to be split by at least 60 µm. This can be achieved by a combination of two biprism and a focusing lens, a setup accomplished with electrons in [51].

small distance outside of the coil and far away from the coil endings, the magnetic field equals approximately zero. For that reason no Lorentz force will act on the electron partial waves, being separated by the biprism and passing the coil to the left and to the right. The circularly surrounding vector potential $\vec{A}$ however does have a nonzero value outside the coil, $A_\varphi = \frac{\Phi}{2\pi r}$, with the magnetic flux $\Phi = B\pi R^2$, the radial distance from the border of the coil r and the coil radius R. By variation of the coil current it is possible to continuously vary the vector potential, which points in opposite directions for the separated electron wave paths and causes a different phase shift. After combining the partial waves in the detection plane, the effect is visible in a total phase shift of the interference pattern [45]:

$$\Delta\Phi_{mag} = \frac{e}{\hbar}\oint \vec{A}\cdot d\vec{s} = \frac{e}{\hbar}\Phi = \frac{e}{\hbar}\cdot B\pi R^2 = \frac{e}{\hbar}\cdot \mu_0 \frac{N}{L} I \cdot \pi R^2 \quad . \tag{2}$$

In the previous experiments concerning the magnetic Aharonov-Bohm effect [46, 48, 49, 50] this influence of the vector potential was only measured for structureless particles, namely electrons. In [47] it was pointed out, that there is potentially a different behaviour of ions in this experiment compared to electrons due to spin-orbit interactions. This issue is still in discussion, since concrete experiments are yet absent. Additionally, an experiment is proposed in [47], where the separated ion waves are coherently excited to two internal states by a laser in combination with a microwave

generator. The setup is therefore similar to the one in Fig. 8 a), but with a laser and microwave excitation of the ions in both interferometer arms after the beam was splitted. The particles are measured either directly on the detector or by collecting the fluorescent light emitted through the transition to the ground state. It could be shown theoretically [47], that under specific circumstances the Aharonov-Bohm effect is only visible in the phase of the oscillation in the optical fluorescence signal and not in the spatial interference pattern on the detector. Such an experiment makes it feasible to add an additional phase to the oscillation between two internal ionic states, that originates from the vector potential.

In the context of recently published interference experiments with large, neutral biomolecules with diameters up to 60 Å [14], the interesting question arises, how the spatial extension of a large charged molecule will change the phase shift in the magnetic Aharonov-Bohm effect. The de Broglie wavelength of the ion, $\lambda = \frac{h}{p}$, depends on the canonical momentum $\vec{p} = m\vec{v} - e\vec{A}$, where the vector potential $\vec{A} = \vec{A}(\vec{r})$ depends on the distance from the coil, which is different for different sides of a large molecule. The question arises, if this would cause a dephasing of the resulting interference pattern, or if the effect averages out, due to the longer interaction time further away from the coil center.

4.2. The electrostatic Aharonov-Bohm effect

Besides the magnetic effect, Aharonov and Bohm described a similar experiment, where a scalar potential influences the phase difference between two electron waves [45]. As it is illustrated in fig. 9 a), the two coherent partial waves, separated by the biprism, propagate through two tiny metal cylinders. Inside the tubes, the particles are shielded against any fields from outside. In the original idea of Aharonov and Bohm, an electron source is pulsed to emit wave packages smaller than the length of the metal cylinders. As soon as the wave packages are inside the cylinders, electrostatic potentials will be applied on those tubes with the difference V. They will be set to zero before the electrons leave the cylinders. Thereby the electrons are exposed to scalar potentials, but not to an electrical field. This causes also a different phase shift of the partial waves, which can be observed in a shift of the interference pattern in the detector by

$$\Delta\Phi_{el} = \frac{e}{\hbar}\int V dt \quad . \tag{3}$$

The reason why this original proposal of Aharonov and Bohm could not be verified directly to date in the experiment is the high velocity of the electrons in the interferometer. Under normal conditions in a biprism interferometer experiment, the electrons get emitted by the metal tip with energies between 0.5 and 10 keV. Lower emission energies could in principle be realized by slowing down the electrons with a counter electrode, but due to charging effects and electromagnetic noise it gets more and more demanding to control the beam and maintain coherence.

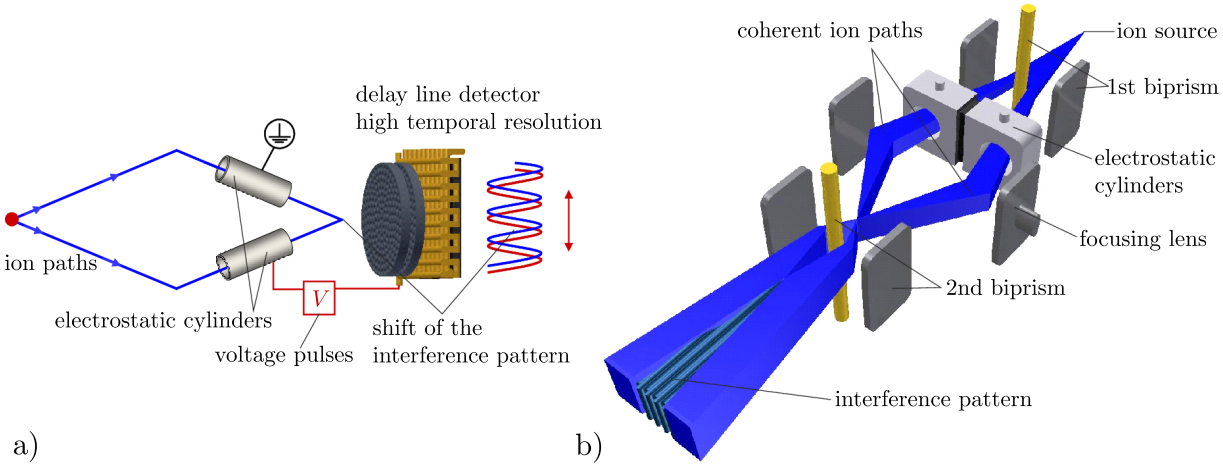

Figure 9. (Color online) Proposed proof of the electrostatic Aharonov-Bohm effect with ions. a) The coherent ion beam gets separated by a biprism into two paths, both passing metal tubes (electrostatic cylinders). Applying a short voltage pulse on one of them, whereas the other one is grounded, shifts the phase of the interference pattern of those ions, that have been inside the cylinders during the pulse. This signal can be isolated due to the good time resolution of the delay line detector, which is correlated with the cylinder pulses. b) Proposed experimental realization with ions. The beam path separation needs to be $\sim 250\,\mu$m to insert two electrostatic cylinders between the partial waves. In the setup that should allow to observe the electrostatic Aharonov-Bohm effect, this can be achieved by a combination of two biprism and a focusing lens, which was accomplished for electrons in [51].

With a typical emission energy of 1 keV, electrons have a velocity of $\sim 2 \times 10^7$ m/s. Under realistic experimental conditions, the maximal length of a tube inserted into the beam path was determined to be 3 mm [51]. The electrons spend only a time of ~ 160 ps in such a cylinder. This is too short to apply a full voltage pulse on one of the cylinders. With ions the situation is more comfortable. A strong beam of hydrogen dimers H_2^+ can be emitted from a SAT at a voltage of 3.8 kV [5]. This corresponds to an ion velocity of only $\sim 6 \times 10^5$ m/s, due to the larger mass compared to electrons. The hydrogen ions would therefore spend a time of 5 ns in a 3 mm cylinder. Voltage pulses with widths around 1 ns are feasible to create with modern pulse generators. Using on the contrary electrons with such a low velocity, they need to be slowed down to ~ 1 eV, which is experimentally to date not possible in a biprism interferometer setup. For that reason, the modified ion interferometer described in this article, would be the ideal candidate for the first direct proof of the electrostatic Aharonov-Bohm effect. However, it needs to be pointed out, that it is necessary to separate the beam to a larger extend as for the situation in fig. 1, where only one biprism is installed. Such a modification will be discussed in the next section.

4.3. Large beam path separation

To measure the two Aharonov-Bohm effects with the biprism ion interferometer, it is required to change the setup. The path separation needs to be increased far enough to install a micro-coil or two metal cylinders in between the beam paths. For a technically feasible realization for the micro-coil, this separation has to be at least 60 µm. This can be achieved by a combination of two biprism or one biprism and a focusing lens. Several different configurations have been studied with electron interferometers to fulfill this task [17, 46, 51]. The largest beam path splitting distance was achieved for electrons with a scheme shown in fig. 8 b) and fig. 9 b). Thereby the beam was separated by $\sim 300\,\mu m$ [51].
We propose to apply this method in the modified ion interferometer. Thereby the first, positively charged biprism splits up the coherent ion beam in two divergent partial waves. The distance of the beam separation can be adjusted by the voltage applied to this biprism. Subsequently the beam gets focussed by a positively charged ion lens. After the beams cross each other, they propagate divergently towards the second biprism, which is negatively charged. It overlaps and interferes the beam paths in the detection plane. The advantage of such a setup is, that the distance between the detected interference maxima is independent of the beam path separation in the area between the first biprism and the focusing lens. The interference pattern can therefore be optimized on detection parameters, such as the magnifying quadrupol lenses and the detector resolution, without changing the distance between the beam path and the object (coil, cylinder) in the interferometer.

4.4. Measurement of the magnetic Aharonov-Bohm effect with ions

The phase shift due to the vector potential of a magnetic coil is not dependent on the mass or the velocity of the particle, as shown in eq. 2. It should therefore be the same for ions and electrons. With a biprism interferometer and a beam path separation scheme as described above, this effect was measured for electrons in [51]. They implemented a micro-coil with a wire thickness of 7 µm, a length of 50 mm and a diameter of 37.5 µm and measured a phase shift of 2π for a current difference in the coil of 55 µA. The measurement error compared to the outcome of eq. 2 was only 4 %.
Based on these values and with the modified ion interferometer, as described above with a high signal count rate, we propose an experiment to measure the magnetic Aharonov-Bohm effect for particles with inner structure, such as helium and hydrogen ions. This proof of principle quantum optical approach should address the questions still under discussion concerning the dependence of the internal structure in the magnetic Aharonov-Bohm effect.

4.5. Measurement of the electrostatic Aharonov-Bohm effect with ions

According to eq. 3, the phase shift of the charged particle wave due to the electrostatic Aharonov-Bohm effect depends on the time, the partial waves are exposed to different scalar potentials. As described above and in fig. 9, the shift is therefore dependent on the voltage pulse length applied on the metal cylinder. The pulse length is constraint by the velocity of the particles and the length of the cylinder. A realistic experiment can only be performed with ions and not, as proposed originally by Aharonov and Bohm [45], with electrons, since they are too fast. For that reason we propose the first direct proof of the electrostatic Aharonov-Bohm effect with hydrogen ions in the modified ion interferometer with the large beam separation by two biprism. The setup is shown in Fig. 9 b).
Aharonov and Bohm suggested a pulsed source. This is in principle possible by irradiating a pulsed femtosecond laser on a high voltage field emission tip. Such a source setup was realized in [52] and emits femtosecond pulses of free electrons. It is conceivable, that this scheme also works for ion emission from a SAT at lower pulse rates. But it is experimentally more convenient to keep the ion emission continuous and perform a temporal selection of the ion events in the detector. By triggering the detector with the pulses on the cylinder, it counts only those ions, that have been inside the metal tubes when the electrostatic potential, therefore the voltage pulse, was switched on. Certainly, with pulse duration times of a few nanoseconds, the time resolution of the detector needs to be in the same range. This is feasible with the modern delay line detector [53] applied in the modified ion interferometer. Temporal resolutions of about one nanosecond are standard in such devices.

To estimate the interference signal which can be expected in such an experiment, we start with the maximal hydrogen signal of $\sim 2.7 \times 10^4$ ions per second, as calculated in section 3.1.1. With a total distance between the source and the detector of 57 cm and a velocity of 6×10^5 m/s an ion spends $\sim 1\,\mu$s inside the beam path. If we pulse the cylinder with 1 MHz, we assure that every ion encounters only one pulse during that time. When this pulse is applied, only in a few cases the ion is inside the cylinder and therefore recorded by the detector. This fraction is given by the cylinder length (3 mm) divided by the length of the interferometer (57 cm). Therefore ~ 140 ions per second are counted by the detector. For a good signal to noise ratio, about 2×10^4 ions are needed for an interferogram [3]. The integration time for one pattern at a specific cylinder-voltage would therefore be around 140 seconds. From [1, 2, 3, 4] we know, that the interferometer is stable enough to integrate the signal for at least 15 minutes. A measurement of the phase shift due to the electrostatic Aharonov-Bohm effect is therefore possible.
In the ion interferometer of Maier et al. a helium partial pressure of 10^{-4} mbar was applied [3]. Such a high pressure is in principle conceivable also in the modified interferometer and would increase the signal for hydrogen by a factor of ten. However, it

may also causes a large background and leads to a high risk of electric discharges in the gas which could destroy the MCPs of the detector.

The expected phase shift depends on the voltage difference between the two cylinders and on the pulse width. The time of flight through the metal cylinders is about 5 ns. Assuming a pulse width of 400 ps, which can be produced by commercially available pulse generators, yields a phase shift of π with a voltage difference of $\sim 5\,\mu$V. The latter value is rather low, it will therefore be a technical challenge to decrease the fluctuations of the voltage pulses down to the µV regime. The introduction of the tiny cylinders is a simpler task. With a beam separation of 250 µm, two cylinders could be installed into the beam paths with an outer diameter of 240 µm and an inner diameter of 70 µm. Such metal tubes are commercially available, since they are produced for medical cannulas.

5. Conclusion

Interferometry experiments with ions are a highly promising platform for fundamental physical tests in quantum optics, in particular in the context of Aharonov-Bohm physics, since ions have charge and internal structure. This features yield several advantages compared to the well established neutral atom, molecular or electron matter wave setups. In this article we discussed major modifications in the first ion interferometer realized by Maier et al. [1, 2, 3, 4] that will permit novel interferometry experiments only accessible for ions. A new regime in Aharonov-Bohm physics could be entered, allowing the measurements of potential structural influences to the Aharonov-Bohm phase or the first direct measurement of the electrostatic Aharonov-Bohm effect.

Until now only one ion interference pattern has been published for 3 kV helium ions [1, 2, 3, 4]. Due to deficiencies in the ion source in this interferometer of Maier et al., rather low coherent ion count rates and long integration times were encountered, which limited the data quality. These deficiencies did not allow sophisticated future experiments. Here we described in detail new developments and improvements of the components in the ion interferometer of Maier et al. and made estimations of the expected performance. Especially new tools for the ion beam generation, such as the SAT, promise a coherent ion signal enhancement by two to three orders of magnitude. We provided a comparison of important beam emission features with other electron and ion sources, indicating the superior properties of the SAT field emission. The use of such sources in the modified interferometer will allow short integration times of potentially a few seconds for high contrast interference patterns. This reduces the requirements for vibrational damping of the apparatus to prevent dephasing and further influences such as noise from the detector and the other electronic devices. With a novel delay line MCP detector, single ions can be measured with high spatial and temporal resolution. The latter can be used to suppress the influences of long term drifts of the interference pattern, yielding a higher contrast. The temporal resolution is also an important con-

dition to prove the electrostatic Aharonov-Bohm effect.
In the original ion interferometer setup of Maier et al. [3], the coherent matter wave beam splitter was realized by an electrostatic biprism, manufactured by manual fiber drawing and subsequent sputtering of a gold-palladium surface. To minimize the fiber-diameter uncertainty in the modified version of the ion interferometer, the biprism wire was manufactured from a standard optical fiber in a highly controlled and reproducible heat-and-pull process. The resulting silica nanowire was then coated with a thin gold layer, yielding a biprism wire with a diameter of about 400 nm and a length of 6 mm.

For the measurement of the magnetic and electrostatic Aharonov-Bohm effect, a scheme for beam path separation up to 250 µm needs to be installed in the ion interferometer to place a magnetic coil or two metal cylinders between the matter waves. A combination of two biprism together with a focusing lens turns out to be optimal. We provided detailed calculations concerning the parameters and the coherent signal strength to be expected in these future experiments.

Besides fundamental approaches such as the Aharonov-Bohm effects, the described enhancements of the ion interferometer potentially allow for even more complex experiments with molecular ions or decoherence experiments with ions close to surfaces [17]. The introduced interferometer is optimized for helium and hydrogen ions but can in principle be expanded to interfere particles with significantly higher masses, e.g. organic molecules. Also technical applications such as high precision sensors and gyroscopes are conceivable [18]. The combination of charge and inner structure, an inherent feature of ions, combines the advantages in interferometry with electrons and neutral atoms. It opens the door for a new class of novel quantum optical experiments.

6. Acknowledgements

We acknowledge Franz Hasselbach for the support and the fruitful discussions. We also thank Uwe Maier for his contribution. We acknowledge the support by the Deutsche Forschungsgemeinschaft (DFG, German Research Foundation) through the Emmy Noether program STI 615/1-1.

References

[1] Hasselbach F and Maier U 1999 Quantum Coherence and Decoherence - Proc. ISQM-Tokyo 98 ed. by Ono Y A and Fujikawa K (Amsterdam: Elsevier) 299-302
[2] Hasselbach F and Maier U 1996 Quantum Coherence and Decoherence ed. by Ono Y A and Fujikawa K (Amsterdam: Elsevier) 69-72
[3] Maier U 1997 Dissertation, University of Tübingen
[4] Hasselbach F 2010 Rep. Prog. Phys. **73** 016101
[5] Kuo H S, Hwang I S, Fu T Y, Lu Y H, Lin C Y and Tsong T T 2008 Appl. Phys. Lett. **92** 063106
[6] Carnal O and Mlynek J 1991 Phys. Rev. Lett. **66** 2689-2692
[7] Keith D W, Ekstrom C R, Turchette Q A and Pritchard D E 1991 Phys. Rev. Lett. **66** 2693-2696

[8] Gustavson T L, Bouyer P and Kasevich M A 1997 Phys. Rev. Lett. **78** 2046-2049
[9] Peters A, Chung K Y and Chu S 1999 Nature **400** 849-852
[10] Grisenti R E, Schöllkopf W, Toennies J P, Hegerfeldt G C, Köhler T and Stoll M 2000 Phys. Rev. Lett. **85** 2284-2287
[11] Brezger B, Hackermüller L, Uttenthaler S, Petschinka J, Arndt M and Zeilinger A 2002 Phys. Rev. Lett. **88** 100404
[12] Rasel E M, Oberthaler M K, Batelaan H, Schmiedmayer J and Zeilinger A 1995 Phys. Rev. Lett. **75** 2633-2637
[13] Gerlich S et al. 2007, Nature Physics **3** 711-715
[14] Gerlich S, Eibenberger S, Tomandl M, Nimmrichter S, Hornberger K, Fagan P J, Tüxen J, Mayor M and Arndt M 2011 Nature Comm. **2** 263
[15] Andrews M R, Townsend C G, Miesner H J, Durfee D S, Kurn D M and Ketterle W 1997 Science **275** 637-641
[16] Krenn G 1999 Dissertation, Technical University Vienna
[17] Sonnentag P and Hasselbach F 2007 Phys. Rev. Lett. **98** 200402
[18] Clauser J F 1988 Physica B **151** 262-272
[19] Nicklaus M 1989 Dissertation, University of Tübingen
[20] Möllenstedt G and Düker H 1956 Z. Phys. A - Hadrons and Nuclei **145** 377-397
[21] Hasselbach F 1988 Z. Phys. B - Condensed Matter **71** 443-449
[22] Kuo H S, Hwang I S, Fu T Y, Lin Y C, Chang C C and Tsong T T 2006 Japanese J. Appl. Phys. **45** 8972-8983
[23] Fu T Y, Cheng L C, Nien C H and Tsong T T 2001 Phys. Rev. B **64** 113401
[24] Warken F, Rauschenbeutel A and Bartholomäus T 2008 Photonics Spectra **42(3)** 73
[25] Warken F, Vetsch E, Meschede D, Sokolowski M and Rauschenbeutel A 2007 Optics Express **15** 11952-11958
[26] Warken F 2007 Dissertation, Technical University Vienna
[27] Stiebeiner A, Garcia-Fernandez R and Rauschenbeutel A 2010 Optics Express **18** 22677-22685
[28] Nicklaus M and Hasselbach F 1993 Phys. Rev. A **48** 152-160
[29] Stefanov A, Zbinden H, Gisin N and Suarez A 2003 Phys. Rev. A, **67** 042115
[30] Wollnik H 1987 *Optics of charged particles* (Orlando: Academic Press)
[31] Hawkes P W and Kasper E 1989 *Principles of electron optics (Basic geometrical optics)* (London and San Diego: Academic Press)
[32] Stibor A, Hornberger K, Hackermüller L, Zeilinger A and Arndt M 2005 Laser Physics **15** 10-17
[33] Reimer L 1998 *Scanning Electron Microscopy: Physics of Image Formation and Microanalysis* (Heidleberg: Springer)
[34] Kalbitzer S and Knoblauch A 2004 Appl. Phys. A **78** 269-281
[35] Kuo H S, Hwang I S, Fu T Y, Hwang Y S, Lu Y H, Lin C Y, Hou J L and Tsong T T 2009 Nanotechnology **20** 335701
[36] Knoblauch A, Wilbertz C, Miller T and Kalbitzer S 1996 J. Phys. D: Appl. Phys. **29** 470
[37] Börret R, Jousten K, Böhringer K and Kalbitzer S 1988 J. Phys. D: Appl. Phys. **21** 1835-1837
[38] Ishikawa T, Urata T, Cho B, Rokuta E and Oshima C 2007 App. Phys. Lett. **90** 143120
[39] Kuo H A, Hwang I S, Fu T Y, Wu J Y, Chang C C and Tsong T T 2004 Nano Lett. **4** 2379-2382
[40] Wilbertz C, Maisch T, Hüttner D, Böhringer K, Jousten K and Kalbitzer S 1992 Nucl. Instr. Meth. Phys. Research Section B: Beam Interactions with Materials and Atoms **63** 120-124
[41] Tsong T T 1990 *Atom-Probe Field Ion Microscopy, Field Ion Emission and Surfaces and Interfaces at Atomic Resolution* (Cambridge and New York: Cambridge University Press)
[42] Block R 1998 Diploma thesis, University of Tübingen
[43] Jousten K, Böhringer K, Börret R and Kalbitzer S 1988 Ultramicroscopy **26** 301-312
[44] Miller T, Knoblauch A, Wilbertz C and Kalbitzer S 1995 Appl. Phys. A **61** 99-100
[45] Aharonov Y and Bohm D 1959 Phys. Rev. **115** 485-491
[46] Möllenstedt G and Bayh W 1962 Naturwissenschften **49** 81-82

[47] Silverman M P 1993 Phys. Lett. A **182** 323-329
[48] Chambers R G 1960 Phys. Rev. Lett. **5** 3-5
[49] Tonomura A, Osakabe N, Matsuda T, Kawasaki T, Endo, J Yano S and Yamada H 1986 Phys. Rev. Lett. **56** 792-795
[50] Batelaan H and Tonomura A 2009 Physics Today **62** 38-43
[51] Schmid H 1985 Dissertation, University of Tübingen
[52] Hommelhoff P, Sortais Y, Aghajani-Talesh A and Kasevich M 2006 Phys. Rev. Lett. **96** 077401
[53] Jagutzki O, Mergel V, Ullmann-Pfleger K, Spielberger L, Spillmann U, Dörner R and Schmidt-Böcking H 2002 Nucl. Instr. Meth. Phys. Research Section A: Accelerators, Spectrometers, Detectors and Associated Equipment **477** 244-249